

# Stationary viscosity-dominated electrified capillary jets

By F. J. HIGUERA

E. T. S. Ingenieros Aeronáuticos, Pza. Cardenal Cisneros 3, 28040 Madrid, Spain

(Received 17 November 2005 and in revised form 17 March 2006)

Numerical computations and order-of-magnitude estimates are used to describe the stationary creeping flow of a jet of a Newtonian liquid with finite electrical conductivity that is injected into a dielectric medium subject to a uniform electric field. The electric current carried by the jet is computed as a function of the parameters of the problem, showing that it increases with the conductivity and flow rate of the liquid and with the intensity of the electric field. The current also depends on the wetting conditions of the liquid at the injection orifice. Analysis of the transfer of current to the surface of the liquid and of the evolution of the jet under the electric stresses that act at its surface leads to scaling laws for the electric current and other properties of the solution. These laws fit the numerical results and are in qualitative agreement with experimental data.

---

## 1. Introduction

When a jet of an electrically conducting liquid is injected through a nozzle into a dielectric medium subject to an electric field, the field induces a conduction current in the liquid that carries electric charge to its surface. The action of the field on this charge leads in turn to an electric shear that stretches the jet and may reduce its diameter to values which are orders of magnitude smaller than the diameter of the injecting nozzle. This mechanism is put to use in electrosprays, where sprays of fine and nearly monodisperse drops are produced by the breakup of an electrified jet due to a varicose instability, and also in the electrospinning of nanofibres, where the jet is made of a polymer solution or melt that solidifies after intense stretching but before it may break into drops (see Fong & Reneker 2000; Yarin 2003; Frenot & Chronakis 2003 and Huang *et al.* 2003 for recent reviews). In this latter application, most of the stretching occurs during the growth of a bending instability whereby the jet begins to spiral violently at some distance downstream of the nozzle. This instability, which determines the final diameter of the fibre, has been documented by Reneker *et al.* (2000) and Yarin, Koombhongse & Reneker (2001) and analysed by these authors and by Shin *et al.* (2001) and Hohman *et al.* (2001a).

The development of the varicose or bending instability is preceded by a region where the jet is stationary and axisymmetric, at least if the viscosity of the liquid is sufficiently high. This initial region is of interest because it contributes to the stretching of the jet, controls the onset and character of the instability, and determines the electric current carried by the jet as a function of the liquid properties and the flow rate. The flow in the initial region is the subject of the present paper. In an asymptotic analysis of the problem, Kirichenko *et al.* (1986) found that the radius of an axisymmetric jet of a Newtonian liquid in a uniform electric field decreases as the power  $-1/4$  of the streamwise distance far away from the nozzle, while Spivak & Dzenis (1998) generalized this result for non-Newtonian liquids with power-law rheologic constitutive

equations. The evolution of the jet before entering this asymptotic regime was computed by Hohman *et al.* (2001*b*) using a quasi-unidirectional model for the flow and charge transport (see Gañán-Calvo 1997) coupled with a slender-body approximation for the electric field induced by the charge of the jet and the image charges on the electrodes. Feng (2002) simplified the computation of the electric field, thereby avoiding an artificial bulging of the jet at the nozzle exit in the results of Hohman *et al.*, and extended these results to include effects of extensional thinning, extensional thickening, and strain hardening, which are beyond the Newtonian liquid model of Hohman *et al.* A shortcoming of these computations is that they do not determine the electric current carried by the jet.

A different approach was taken by Reznik *et al.* (2004), who computed the transient and steady shapes of the surface of a drop of a Newtonian liquid of infinite electrical conductivity sitting on a metallic plate by using boundary element methods to solve the Laplace and Stokes equations that govern the flow in the absence of inertial effects. Their results are extended here to liquids of finite electrical conductivity, as this property appears to be crucial to achieve stationary solutions. The simplest case of a creeping flow of a Newtonian liquid issuing into a region where the electric field would be uniform in the absence of the jet is discussed. An attempt is made to describe the solution of this problem, which depends on five dimensionless parameters, using numerical computations and order-of-magnitude estimates.

## 2. Formulation

Consider a constant flow rate  $Q$  of a Newtonian liquid of viscosity  $\mu$ , surface tension  $\gamma$ , electrical conductivity  $K$ , and permittivity  $\epsilon_0\epsilon$  that is injected into a dielectric medium of permittivity  $\epsilon_0$  through a circular orifice of radius  $a$  drilled through a plate electrode. A high voltage is applied between this electrode and another distant parallel electrode, which leads to a uniform field  $E_\infty$  far from the orifice. Let  $\mathbf{E}^l$  and  $\mathbf{E}$  denote the electric fields in the liquid and in the dielectric medium, which, in the absence of a magnetic field, are of the form  $\mathbf{E}^l = \nabla\phi^l$  and  $\mathbf{E} = \nabla\phi$ , where  $\phi^l$  and  $\phi$  are the negative of the electric potentials. The field  $\mathbf{E}^l$  induces a density of current given by Ohm's law  $\mathbf{j} = K\mathbf{E}^l$ , while charge conservation requires  $\nabla \cdot \mathbf{j} = 0$  in the absence of net electric charge in the bulk of the liquid (Landau & Lifshitz 1960). This condition reduces to  $\nabla \cdot \mathbf{E}^l = 0$  for a liquid of uniform conductivity. Similarly,  $\nabla \cdot \mathbf{E} = 0$  in the dielectric surrounding the liquid. The electric potentials therefore satisfy  $\nabla^2\phi = \nabla^2\phi^l = 0$ , which are to be solved with the boundary conditions  $\epsilon_0(E_n - \epsilon E_n^l) = \sigma$  and  $E_t = E_t^l$  at the surface of the liquid,  $\phi = \phi^l = 0$  at the plate electrode, and the condition that the electric field should tend to  $E_\infty$  away from the electrode. Here  $\sigma$  is the density of free surface charge and the subscripts  $n$  and  $t$  denote the components of the electric fields normal and tangent to the surface, with the normal pointing away from the liquid.

Electric conduction in the liquid brings electric charge to its surface at a rate  $KE_n^l$  per unit area and time. This charge is advected by the flow, leading to a convective electric current which adds to the conduction current. The conservation equation for the surface charge is (Saville 1997)

$$\frac{D\sigma}{Dt} = KE_n^l + \sigma \mathbf{n} \cdot \nabla \mathbf{v} \cdot \mathbf{n}, \quad (2.1)$$

where  $D\sigma/Dt = \partial\sigma/\partial t + \mathbf{v} \cdot \nabla\sigma$  is the material derivative at the surface,  $\mathbf{v}$  is the velocity of the liquid, and the second term on the right is the effect of the surface straining.

The accumulation of charge at the surface tends to screen the liquid from the outer field in a time of the order of the electric relaxation time  $t_e = \epsilon_0 \epsilon / K$ . This characteristic time is derived from the order-of-magnitude balance of the terms  $\partial \sigma / \partial t$  and  $K E_n^l$  in (2.1) taking  $\sigma = O(\epsilon_0 \epsilon E_n^l)$ , which is the condition for the surface charge to have an effect in the boundary condition  $\epsilon_0(E_n - \epsilon E_n^l) = \sigma$  at the liquid surface.

The electric field and the surface electric charge lead to an electric stress at the surface of the liquid whose components normal and tangent to the surface ( $\tau_n^e$  and  $\tau_t^e$ , respectively) are given in dimensionless form by the right-hand sides of (2.5a, b) (Landau & Lifshitz 1960; Saville 1997). It is through this stress that the electric field affects the flow of the liquid.

The inertia of the liquid will be neglected and the surrounding dielectric will be assumed to be a uniform-pressure medium which does not participate in the dynamics of the liquid. The latter assumption is appropriate when the outer medium is a vacuum, or a gas, or a liquid much less viscous than the liquid injected through the orifice. The effect of the inertia of the liquid in the region around the orifice is measured by the Reynolds number  $\rho Q / \mu a$ , where  $\rho$  is the density of the liquid. This Reynolds number is of order  $10^{-2}$  in the experiments of Hohman *et al.* (2001b) with glycerol and PEO solutions, and down to  $3 \times 10^{-4}$  in the experiments of Jayasinghe & Edirisinghe (2004) with silicone oils. Thus, although the Reynolds number of the flow increases in the electrically stretched jet (see the estimate following (2.12) below), the effect of the inertia is small in a long leading region of the jet in many cases of interest.

In what follows, the radius of the orifice  $a$  and the viscous-capillary velocity  $v_c = \gamma / \mu$  are used as scales of length and velocity, and  $E_c = (\gamma / \epsilon_0 a)^{1/2}$ ,  $E_c a$ ,  $\epsilon_0 E_c$ , and  $K E_c a^2$  are used as scales of electric field, electric potential, surface density of charge, and electric current, respectively. The following dimensionless parameters appear:

$$Ca = \frac{\mu Q}{\gamma a^2}, \quad B_E = \frac{\epsilon \epsilon_0 E_c^2 a}{\gamma}, \quad \epsilon, \quad T = \frac{\mu K a}{\epsilon \epsilon_0 \gamma}, \quad \theta, \quad (2.2)$$

which are a capillary number, an electrical Bond number, the dielectric constant of the liquid, the ratio of the residence time  $t_r = a / v_c$  to the electric relaxation time discussed above, and the contact angle of the liquid with the electrode.

The dimensionless equations governing the flow are

$$\nabla \cdot \mathbf{v} = 0, \quad 0 = -\nabla p + \nabla^2 \mathbf{v}, \quad \nabla^2 \varphi^l = 0 \quad (2.3)$$

in the liquid, and

$$\nabla^2 \varphi = 0 \quad (2.4)$$

outside the liquid. These equations are to be solved with the boundary conditions

$$-p + \mathbf{n} \cdot \boldsymbol{\tau}' \cdot \mathbf{n} + \nabla \cdot \mathbf{n} = \frac{1}{2} [E_n^2 - \epsilon E_n^{l2} + (\epsilon - 1) E_t^2], \quad \mathbf{t} \cdot \boldsymbol{\tau}' \cdot \mathbf{n} = \sigma E_t, \quad (2.5a, b)$$

$$E_n - \epsilon E_n^l = \sigma, \quad E_t = E_t^l, \quad \frac{D\sigma}{Dt} = \epsilon T E_n^l + \sigma \mathbf{n} \cdot \nabla \mathbf{v} \cdot \mathbf{n} \quad (2.6a, b, c)$$

at the liquid surface, which is a material surface,

$$\mathbf{v} = \begin{cases} Ca/\pi & \text{for } r < 1, \\ 0 & \text{for } r > 1, \end{cases} \quad \varphi = \varphi^l = 0 \quad (2.7a, b)$$

at the electrode ( $x = 0$ ), and

$$\nabla \varphi = \nabla \varphi^l = \left( \frac{B_E}{\epsilon} \right)^{1/2} \mathbf{i} \quad (2.8)$$

far from the electrode. Here  $p$  is the pressure of the liquid referred to the pressure of the surrounding medium and non-dimensionalized with  $\mu v_c/a$ ;  $\boldsymbol{\tau}'$  is the dimensionless viscous stress tensor, given by the Navier–Poisson law;  $\mathbf{n}$  and  $\mathbf{t}$  are unit vectors normal and tangent to the surface;  $x$  and  $r$  are the dimensionless distances to the plate electrode through which the liquid is injected and to the axis of the injection orifice; and  $\mathbf{i}$  is a unit vector normal to the electrode. Conditions (2.5) are the balances of stresses normal and tangent to the surface. The last term on the left-hand side of (2.5a) is the normal stress due to the surface tension. The inlet flow is assumed to be an equipotential plug flow in (2.7). These conditions are used mostly to simplify the formulation. They can be realized by filling the inlet pipe with a metallic grid.

The surface of the liquid is assumed to be axisymmetric and is sought in the form  $r = r_s(x, t)$ , where  $r_s$ , the radius of the jet cross-section, satisfies

$$\frac{\partial r_s}{\partial t} + v_x \frac{\partial r_s}{\partial x} - v_r = 0. \quad (2.9)$$

Here  $v_x$  and  $v_r$  are the axial and radial components of the velocity of the liquid.

Equations (2.6c) and (2.9) require additional conditions at the contact line of the liquid surface with the electrode. The density of surface charge will be taken to be zero at the contact line, neglecting any charge convected from the Debye layers on the inner walls of the feeding pipe or the electrode (see Hohman *et al.* 2001b; Feng 2002). Two possibilities will be considered for the contact line itself. Either it is unconditionally attached to the edge of the orifice, or it is allowed to drift away from the edge with the liquid surface making a constant contact angle  $\theta$  with the solid electrode. These conditions are

$$r_s = 1 \quad \text{or} \quad \left. \begin{array}{l} \sigma = 0 \\ r_s = 1 \text{ if } -n_x < \cos \theta \\ r_s > 1 \text{ with } -n_x = \cos \theta \text{ otherwise} \end{array} \right\} \quad (2.10)$$

at  $x = 0$ , where  $n_x$  is the axial component of the unit normal to the liquid surface.

In the absence of whipping or breakup, the viscosity-dominated jet would reach an asymptotic quasi-unidirectional regime at large distances from the orifice, where most of the electric current is due to convection of the surface charge and the field tangent to the surface nearly coincides with the applied field. In these conditions  $2\pi\sigma v_x r_s \approx \epsilon T I$ , with  $v_x \approx Ca/\pi r_s^2$ , and  $E_t \approx (B_E/\epsilon)^{1/2}$ , so that the dimensionless electric shear is  $\tau_t^e = \sigma E_t \approx \frac{1}{2}\epsilon T I (B_E/\epsilon)^{1/2} r_s / Ca$  in this far region. On the other hand, the balance of axial forces on a stationary quasi-unidirectional jet (which can be derived from (2.3) and (2.5)) is

$$\frac{\partial}{\partial x} \left( 3\pi r_s^2 \frac{\partial v_x}{\partial x} \right) + \pi r_s^2 \frac{\partial}{\partial x} \left( \tau_n^e - \frac{1}{r_s} \right) + 2\pi r_s \tau_t^e = 0, \quad (2.11)$$

where the three terms are the effective axial viscous force, the force due to the pressure variation induced by the normal electric stress and the surface tension, and the force due to the electric shear. Equation (2.11) differs from the momentum equation of Hohman *et al.* (2001a) and Feng (2002) in that the convective acceleration of the liquid, which leads to a term  $R\partial(\pi r_s^2 v_x^2)/\partial x$  with  $R = \rho a \gamma / \mu^2$ , has been omitted from the left-hand side on the assumption that  $R \ll 1$ . The effect of the normal electric stress becomes negligible far downstream and (2.11) yields

$$r_s \sim \frac{A}{x}, \quad \text{with } A = \frac{\pi}{2} \frac{Ca}{\epsilon T I (B_E/\epsilon)^{1/2}} \left\{ 1 + \sqrt{1 + \frac{24}{\pi} \epsilon T I \left( \frac{B_E}{\epsilon} \right)^{1/2}} \right\}. \quad (2.12)$$

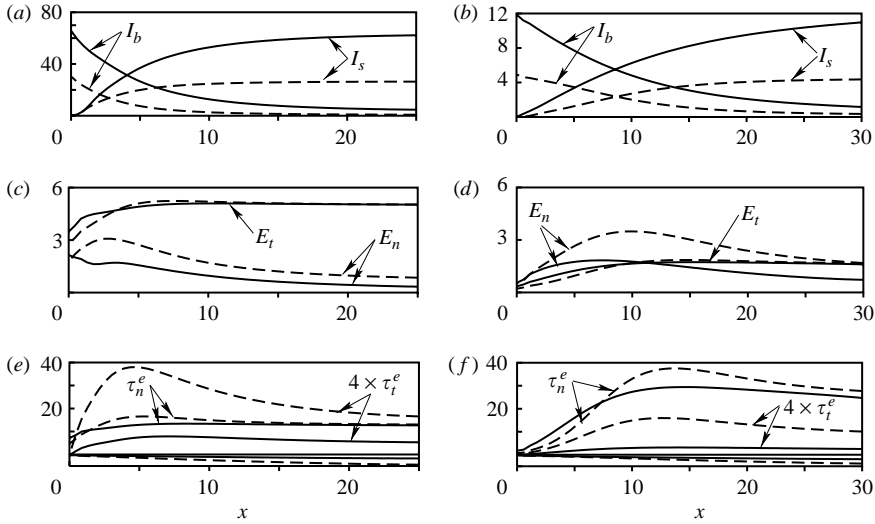


FIGURE 1. Axial distributions of conduction and convection current (first row); electric field normal and tangent to the liquid surface (second row); and normal electric stress ( $\tau_n^e$ ), tangent electric stress ( $\tau_t^e$ ), and surface tension stress ( $-\nabla \cdot \mathbf{n}$ , small, negative, unlabelled curves) (third row). (a, c, e)  $\epsilon = 2$ , and (b, d, f)  $\epsilon = 20$ . The solid curves are for  $T = 2.5$  and the dashed curves for  $T = 50$ .  $Ca = 300$  and  $B_e = 50$  in all the cases.

The convective acceleration of the liquid comes into play for  $x = O[A^{3/2}/R^{1/4}Ca^{1/2}]$ , and the results of Kirichenko *et al.* (1986) would apply further downstream.

Stationary axisymmetric solutions of (2.3)–(2.10) have been computed numerically using standard boundary element methods to solve the Stokes and Laplace equations (2.3) and (2.4) and a second-order Runge–Kutta method to integrate the evolution equations (2.9) and (2.6c) for the liquid surface and surface charge density, and marching in time until the solution becomes stationary.

In typical cases, the numerical solution seems to tend to the downstream asymptotic regime (2.12) only very far from the orifice, making it doubtful that (2.12) will always be attained in real cases, when the jet is subject to bending instabilities and breakup. These complexities are not discussed here and, in order to simplify the computations, the jet is truncated and artificially suppressed beyond a section at a finite distance from the orifice. This drastic approximation replaces (2.12). Numerical tests show that the solution in the region of interest is insensitive to the approximation when the jet is truncated sufficiently far from the orifice. Cutoff distances of 30 to 40 orifice radii suffice for this purpose at the largest dimensionless flow rates discussed below.

### 3. Results and discussion

#### 3.1. Numerical results

The total electric current  $I$  is the sum of the conduction current ( $I_b = 2\pi \int_0^{r_s} r E_x^l dr$ ), which decreases with distance along the jet and tends to zero far downstream, and the surface convection current ( $I_s = 2\pi\sigma v_s r_s / \epsilon T$ ), which is zero at the injection orifice and increases to account for the total current far downstream; see figure 1(a, b). The total electric current is independent of  $x$  and can be computed as part of the solution. It is plotted in figure 2 as a function of the dimensionless flow rate  $Ca$  for different values

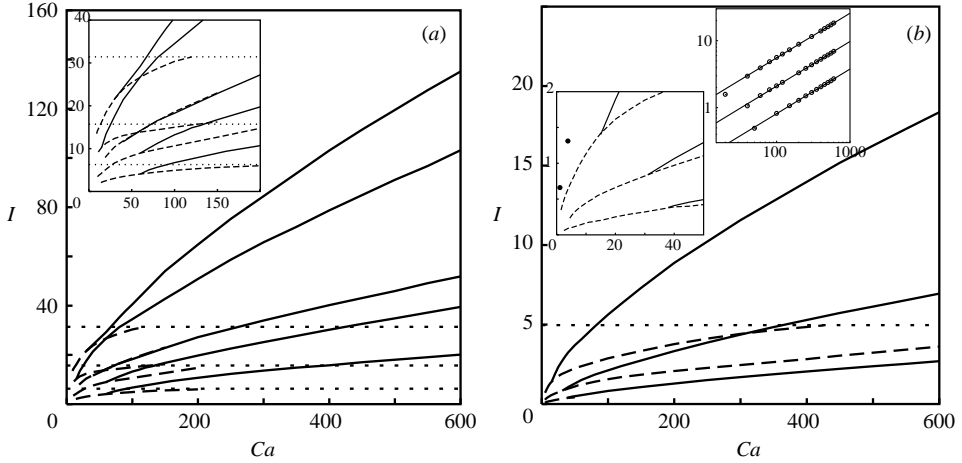


FIGURE 2. Dimensionless electric current (non-dimensionalized with  $KE_c a^2$ ) as a function of the capillary number. The solid curves are for a liquid surface touching the electrode with a contact angle  $\theta = 70^\circ$ , and the dashed curves are for a contact line attached to the edge of the orifice. The five curves in (a), for  $\epsilon = 2$ , are, from bottom to top, for  $(B_E, T) = (8, 50)$ ,  $(50, 50)$ ,  $(200, 50)$ ,  $(50, 2.5)$ , and  $(200, 2.5)$ . In (b), for  $\epsilon = 20$ ,  $B_E = 50$  and  $T = 500, 50$  and  $2.5$ , from bottom to top. The insets show the branching of solid and dashed curves and the smallest  $Ca$  at which stationary solutions have been obtained. The circles in the upper inset of (b) are numerical results and the lines have the slope  $2/3$  predicted by (3.2).

of  $T$ ,  $B_E$  and  $\epsilon$ . The contact line of the liquid surface with the electrode coincides with the edge of the orifice in a range of low  $Ca$  (dashed curves of figure 2). In this range, which is of interest for electrospinning, the jet ceases to be stationary at a distance from the orifice that decreases with  $Ca$  and is about 10 orifice radii at the smallest values of  $Ca$  in figure 2. On approaching these smallest  $Ca$ , the meniscus sometimes displays a rapid contraction which suggests that a jetting-to-dripping transition similar to the transition in the absence of an electric field may occur. Although the numerical code cannot follow the pinchoff and detachment of drops, the stationary solutions show that the onset of dripping depends on the electric field and values of  $\epsilon$  and  $T$ . Appropriate combinations of these parameters should suppress dripping and lead to the cone-jet regime of electrospinning, but this is not investigated here. The two black circles in the left-hand inset of figure 2(b) are experimental results of Hohman *et al.* (2001b) for glycerol ( $\epsilon = 46.5$ ,  $T = 45.6$ ). The comparison with these results is only qualitative because the feeding pipe protrudes from the electrode in the experiments, intensifying the electric field in a manner that is not accounted for in the computations.

The current increases with  $Ca$  but never reaches values much higher than  $I_m = \pi(B_E/\epsilon)^{1/2}$  when the contact line is not allowed to separate from the orifice. This  $I_m$ , which is given by the dotted horizontal lines in figure 2, is the limiting current that would be attained if the effects of the electric shear and the transfer of current to the surface were negligible in the vicinity of the orifice. The cross-section of the jet is then a circle of unit dimensionless radius (for the inlet plug flow used in (2.7a)) and the dimensionless electric field in the liquid is equal to the applied field  $E_\infty/E_c = (B_E/\epsilon)^{1/2}$ . The limiting current is approached and even slightly exceeded by the dashed curves of figure 2 when  $Ca$  increases. The numerical method fails to converge above a certain value of  $Ca$  at which the electric field flips and points toward the liquid.

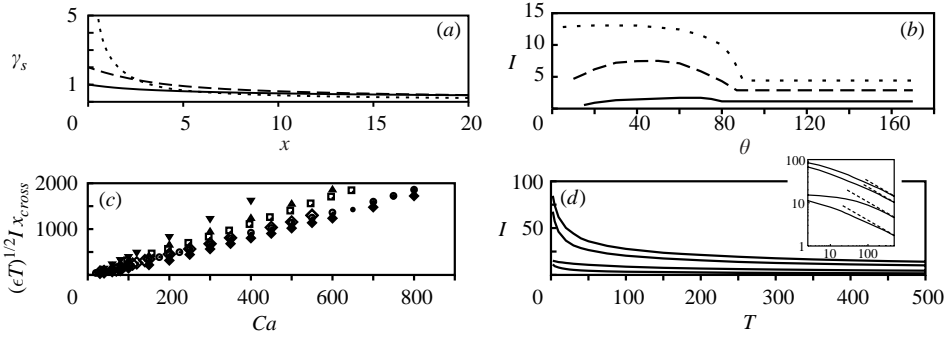


FIGURE 3. (a) Dimensionless radius of the jet as a function of the dimensionless streamwise distance for  $Ca = 100$ ,  $B_E = 50$ ,  $\epsilon = 20$ ,  $T = 2.5$ , and three values of the contact angle:  $\theta = 90^\circ$  (solid),  $70^\circ$  (dashed), and  $10^\circ$  (dotted). (b) Dimensionless electric current (non-dimensionalized with  $KE_c a^2$ ) as a function of  $\theta$  for  $B_E = 50$ ,  $\epsilon = 20$ , and  $(Ca, T) = (300, 50)$  (solid),  $(100, 2.5)$  (dashed), and  $(300, 2.5)$  (dotted). (c) Scaled cross-over distance at which  $I_b(x_{cross}) = I_s(x_{cross})$  as a function of  $Ca$  for  $(\epsilon, B_E, T)$ .  $\circ$ ; (2, 50, 2.5),  $\bullet$ ; (2, 200, 2.5),  $\square$ ; (2, 8, 50),  $\diamond$ ; (2, 50, 50),  $\blacklozenge$ ; (2, 200, 50),  $\blacktriangle$ ; (20, 50, 2.5),  $\blacktriangledown$ ; (20, 50, 2.5). (d) Dimensionless electric current as a function of  $T$  for  $(\epsilon, Ca, B_E) = (2, 300, 200)$ ,  $(2, 300, 50)$ ,  $(2, 100, 50)$ , and  $(20, 300, 50)$ , from top to bottom. The dashed lines in the inset have the slope  $-1/2$  predicted by (3.2).

On the other hand, the electric current increases with  $Ca$  without apparent bound when the contact line is allowed to separate from the orifice. The solid curves of figure 2 are for a surface making a contact angle  $\theta = 70^\circ$  with the electrode, and figure 3(b) shows the evolution of the current with  $\theta$  for given values of the other parameters. Separation of the contact line from the orifice is marked in figure 2 by the branching of the solid curve from the dashed curve for the same set of parameter values. The solid curve is always above the dashed curve because the conduction current across the orifice is augmented by the conduction current that enters the liquid through the wetted region of the electrode when  $r_s(x=0) > 1$ . The area of the wetted region increases when the contact angle decreases (see figure 3a), which explains the initial rise of the current in figure 3(b) with decreasing  $\theta$ . The current goes through a maximum and decreases when  $\theta$  is further decreased because the electric field in the liquid decreases when its surface becomes nearly parallel to the electrode. (Compare the field  $E^l \approx (E_x - \sigma)/\epsilon$  from (2.6a) for a liquid surface parallel to the electrode with  $E^l \approx E_x$  from (2.6b) for a liquid surface perpendicular to the electrode. Here  $E_x$  is the axial field at the outer side of the surface.)

At a given value of  $Ca$ , the dimensionless electric current in figure 1 increases with the applied field  $(B_E/\epsilon)^{1/2}$  and decreases when  $T$  is increased. The effect of  $(B_E/\epsilon)^{1/2}$  is due to the increase of the conduction current at the orifice and the wetted surface of the electrode with the applied field. On the other hand, increasing  $T$  amounts to increasing the rate of transfer of electric charge to the surface. This charge increases the electric shear that stretches the jet (right-hand side of (2.5b)), and the augmented stretching reduces the conduction current by decreasing the cross-section of the jet. In addition, the increase of the surface charge due to the increase of  $T$  favours the screening of the liquid from the applied field. The radius of the jet at a given distance from the orifice is a decreasing function of  $(B_E/\epsilon)^{1/2}$  and  $T$  and increases with  $Ca$ .

The density of free surface charge  $\sigma$  (not displayed) is zero at the electrode, increases with streamwise distance due to the conduction current  $\epsilon T E_n^l$  normal to the surface, reaches a maximum (which increases with  $T$ ) in the current transfer region of the jet

where the bulk conduction and surface convection currents are of the same order, and finally decreases as  $\sigma \sim \epsilon TI/v_x r_s \sim \epsilon T I r_s / Ca$  due to the continuous stretching of the jet when the convection current is already of the order of the total current.

The density of free surface charge and the electric displacement in the liquid add to generate a normal field  $E_n = \sigma + \epsilon E_n^l$  at the outer side of the surface. The computed values of the normal and tangent fields,  $E_n$  and  $E_t$ , are given in figure 1(c, d) as functions of the streamwise distance for a few representative cases. The normal field increases with  $\epsilon$  and  $T$ . It has a maximum at a position that is at or very near the orifice for small values of  $\epsilon$  and  $T$ , and that shifts streamwise when these parameters and  $Ca$  are increased. The numerical results show that  $E_n$  is small compared with  $E_t$  for an apolar liquid ( $\epsilon = 2$ ), except in a region around the orifice where, for  $T = 50$  and relatively small  $Ca$ , the contribution of  $\sigma$  gives a peak  $E_n$  of the order of  $E_t$ . For a polar liquid ( $\epsilon = 20$ ), on the other hand,  $E_n$  is already of the order of  $E_t$  when  $T = 2.5$ , in which case  $\epsilon E_n^l$  is the major contribution to  $E_n$ , and  $E_n$  is somewhat larger than  $E_t$  when  $T = 50$ , in which case the contributions of  $\sigma$  and  $\epsilon E_n^l$  are comparable and peak at about the same place. Even though  $\sigma$  is larger than  $\epsilon E_n^l$  on most of the surface when  $T = 50$ , the contribution of the latter to  $E_n$  becomes negligible only far downstream in the jet, at a distance that increases when  $\epsilon$  or the dimensionless flow rate  $Ca$  increase.

Since increasing  $T$  amounts to decreasing the electric relaxation time, the surface charge is in equilibrium for large values of  $T$ , in the sense that  $\sigma \approx E_n \gg \epsilon E_n^l$  in (2.6a); see e.g. Gañán-Calvo (1997). This does not mean that the surface of the liquid becomes equipotential, as an electric field tangent to the surface still exists to sustain the conduction current carried by the liquid. The tangent field leads to an electric shear at the surface which appears to be crucial to maintain a stationary jet. Computations carried out for a strictly equipotential liquid failed to converge to a stationary state, showing instead a continuous decrease of the jet radius with time until the numerical scheme breaks down.

The outward electric stress (right-hand side of (2.5a)), diminished by the relatively small inward stress due to the surface tension, induces a depression in the liquid (see figure 1(e, f) and the second term of (2.11)). This depression has a maximum, which becomes more pronounced and shifts upstream when  $T$  increases or  $Ca$  decreases, and then slowly decreases, leading to a pressure force that opposes the flow. This force, however, is always smaller than the resultant of the electric shear acting on the perimeter of the jet cross-section (third term of (2.11)), so that the jet is continuously stretched. The continuous stretching stabilizes the jet (Taylor 1969) and probably explains its ability to negotiate the long region where the surface tension is outbalanced by the normal electric stress.

### 3.2. Order-of-magnitude estimations

The characteristic length of the region of the jet where the bulk conduction current is transferred to surface convection current ( $x_r$ , say) can be estimated in terms of the parameters of the problem and the value of the electric current using the following order-of-magnitude balances: (i) the condition  $\sigma v_x r_s \sim \epsilon TI$ , with  $v_x \sim Ca/r_s^2$ , defines the current transfer region; (ii) the condition that the rate of surface charge accumulation (left-hand side of (2.6c)) should be of the order of the conduction current normal to the surface (first term on the right-hand side of (2.6c)) requires  $v_x \sigma / x_r \sim \epsilon T E_n^l$ , where  $E_n^l \sim r_s (B_E / \epsilon)^{1/2} / x_r$  from the divergence-free condition  $\nabla \cdot \mathbf{E}^l = 0$  with  $E_x^l \sim (B_E / \epsilon)^{1/2}$ ; (iii) the balance of axial viscous and electric forces in (2.11), already used to derive (2.12), requires  $r_s^2 v_x / x_r^2 \sim r_s \tau_t^e$ , where  $\tau_t^e \sim \sigma (B_E / \epsilon)^{1/2}$ . These three

balances taken together imply

$$x_T \sim \frac{Ca}{(\epsilon T)^{1/2} I}, \quad r_{sT} \sim \frac{I^{1/2}}{(B_E/\epsilon)^{1/4}}, \quad \sigma_T \sim \frac{\epsilon T I^{3/2}}{Ca(B_E/\epsilon)^{1/4}}, \quad (3.1)$$

where  $r_{sT}$  and  $\sigma_T$  are the characteristic values of the dimensionless jet radius and surface charge density in the current transfer region. This  $\sigma_T$  is an estimate of the maximum surface charge density. The estimates (3.1) are in line with the numerical results. Figure 3(c) shows the distance  $x_{cross}$  to the orifice at which the conduction and convection currents are equal to each other. As can be seen, results for different values of  $\epsilon$ ,  $T$  and  $B_E$  approach a common straight line when the scaling suggested by the first estimate (3.1) is used. The ratio of the normal electric displacement to the surface charge density is  $\epsilon E_n^l/\sigma \sim (B_E/T)^{1/2}$  in the current transfer region, independent of the flow rate and the electric current. The condition of equilibrium of the surface charge is therefore  $T \gg B_E$ .

An estimate of the dimensionless electric current as a function of the parameters of the problem can be obtained noticing that the axial variation of  $E_t$  in figure 1(c, d) reflects that the axial field induced by the charge on the surface of the jet is of the order of the applied field. Since the jet acts as a line of charge, the induced axial field is of order  $E_n r_{sT}/x_T$  with  $E_n \approx \sigma_T$  (see e.g. Ashley & Landahl 1965; Feng 2002), and the condition that this field should be of order  $(B_E/\epsilon)^{1/2}$  gives, upon using (3.1),

$$I \sim \frac{Ca^{2/3}(B_E/\epsilon)^{1/3}}{(\epsilon T)^{1/2}}. \quad (3.2)$$

This estimate should be valid for capillary numbers large compared with the minimum value at which a stationary jet ceases to exist and for values of the other parameters such that the stretching of the jet is large in the current transfer region ( $x_T \gg 1$  and  $r_{sT} \ll 1$ ), in order for (3.1) to apply. The logarithmic plot in the upper inset of figure 2(b) shows that the current follows a  $Ca^{2/3}$  law for  $\epsilon = 20$ ,  $B_E = 50$ , and different values of  $T$ . The inverse square-root dependence of the current on  $T$  is achieved for large values of this parameter, as illustrated in figure 3(d). The predicted power-law dependence on the applied field also seems to occur for large values of the field, though this result is probably less relevant, as long stationary jets should not be expected in large ranges of  $(B_E/\epsilon)^{1/2}$ . In dimensional variables, (3.2) amounts to an electric current proportional to  $\epsilon_0^{1/3} \mu^{1/6} K^{1/2} E_\infty^{2/3} Q^{2/3}$ , which is independent of the surface tension and depends weakly on the viscosity of the liquid.

The estimates (3.1) and (3.2) have been worked out for a uniform applied electric field, which is specific to the parallel-plate electrode configuration. These estimates can be easily adapted to other forms of the electric field far from the orifice (see Higuera 2004 for a similar analysis of the cone-jet regime of an electrospray). Thus for  $E_t \sim 1/x_T^{1/2}$ , which is the electric field of a Taylor cone, (3.2) changes to  $I \sim (Ca/\epsilon T)^{1/2}$ , recovering the square-root dependence of the current on the flow rate which is the hallmark of the cone-jet regime. If  $E_t \sim B/x_T$  with  $B$  constant, which is the field around an isolated needle, then the estimate of the current becomes  $I \sim B^2/(\epsilon T)^{1/2}$ , independent of the flow rate.

#### 4. Conclusions

The creeping flow of a stationary jet of a Newtonian liquid with finite electrical conductivity injected into a uniform electric field through a circular orifice in one of the electrodes creating the field has been described numerically. The flow is driven

mainly by the electric shear due to the action of the electric field on the electric charge that the field itself accumulated at the surface of the liquid. The electric current carried by the jet has been computed and shown to depend on the wetting conditions at the electrode surface. The crucial role of the electric shear at establishing a stationary jet has been confirmed, and the effect of the surface tension has been found to be small in a long region of the jet. Order-of-magnitude estimates have been worked out for the electric current and the properties of the jet in the region where the conduction current is transferred to surface convection current. These estimates provide a physical interpretation of the numerical results.

This work was supported by projects DPI2004-05246-C04-02 (MEC), S-0505/ENE-229 (CM), and R05/9961 (UPM-CM).

#### REFERENCES

- ASHLEY, H. & LANDAHL, M. 1965 *Aerodynamics of Wings and Bodies*, Chap. 6. Addison-Wesley.
- FENG, J. J. 2002 The stretching of an electrified non-Newtonian jet: A model for electrospinning. *Phys. Fluids* **14**, 3912–3926.
- FONG, H. & RENEKER, D. H. 2000 Electrospinning and formation of nanofibers. In *Structure Formation in Polymer Fibers* (ed. D. R. Salem & M. V. Sussman), pp. 225–246. Hauser, Munich.
- FRENOT, A. & CHRONAKIS, I. S. 2003 Polymer nanofibers assembled by electrospinning. *Curr. Opin. Colloid Interface Sci.* **8**, 64–75.
- GAÑÁN-CALVO, A. M. 1997 On the theory of electrohydrodynamically driven capillary jets. *J. Fluid Mech.* **335**, 165–188.
- HIGUERA, F. J. 2004 Current/flow-rate characteristic of an electrospray with a small meniscus. *J. Fluid Mech.* **513**, 239–246.
- HOHMAN, M. M., SHIN, M., RUTLEDGE, G. & BRENNER, M. P. 2001a Electrospinning and electrically forced jets. I. Stability theory. *Phys. Fluids* **13**, 2201–2220.
- HOHMAN, M. M., SHIN, M., RUTLEDGE, G. & BRENNER, M. P. 2001b Electrospinning and electrically forced jets. II. Applications. *Phys. Fluids* **13**, 2221–2236.
- HUANG, Z. M., ZHANG, Y. Z., KOTAKI, M. & RAMAKRISHNA, S. 2003 A review on polymer nanofibers by electrospinning and their applications in nanocomposites. *Composites Sci. Technol.* **63**, 2223–2253.
- JAYASINGHE, S. N. & EDIRISINGHE, M. J. 2004 Electrically forced jets and microthreads of high viscosity dielectric liquids. *J. Aerosol Sci.* **35**, 233–243.
- KIRICHENKO, V. N., PETRIANOV-SOKOLOV, I. V., SUPRUN, N. N. & SHUTOV, A. A. 1986 Asymptotic radius of a slightly conducting liquid jet in an electric field. *Sov. Phys. Dokl.* **31**, 611–614.
- LANDAU, L. D. & LIFSHITZ, E. M. 1960 *Electrodynamics of Continuous Media*. Pergamon.
- RENEKER, D. H., YARIN, A. L., FENG, H. & KOOMBHONGSE, S. 2000 Bending instability of electrically charged liquid jets of polymer solutions in electrospinning. *J. Appl. Phys.* **87**, 4531–4547.
- REZNIK, S. N., YARIN, A. L., THERON, A. & ZUSSMAN, E. 2004 Transient and steady shapes of droplets attached to a surface in a strong electric field. *J. Fluid Mech.* **516**, 349–377.
- SAVILLE, D. A. 1997 Electrohydrodynamics: The Taylor-Melcher leaky dielectric model. *Annu. Rev. Fluid Mech.* **29**, 27–64.
- SHIN, Y. M., HOHMAN, M. M., BRENNER, M. P. & RUTLEDGE, G. C. 2001 Electrospinning: A whipping fluid jet generates submicron polymer fibers. *Appl. Phys. Lett.* **78**, 1149–1151.
- SPIVAK, A. F. & DZENIS, Y. A. 1998 Asymptotic decay of radius of a weakly conductive viscous jet in an external electric field. *Appl. Phys. Lett.* **73**, 3067–3069.
- TAYLOR, G. I. 1969 Electrically driven jets. *Proc. R. Soc. Lond. A* **313**, 453–475.
- YARIN, A. L. 2003 *Electrospinning of Nanofibers from Polymer Solutions and Melts*. Lecture Notes AMAS, No. 5. AMAS Publications, Warsaw.
- YARIN, A. L., KOOMBHONGSE, S. & RENEKER, D. H. 2001 Bending instability in electrospinning of nanofibers. *J. Appl. Phys.* **89**, 3018–3026.